

Space-based retrieval of NO₂ over biomass burning regions: quantifying and reducing uncertainties

N. Bousseréz^{1,*}

¹Dalhousie University, Halifax, N.S., Canada

*now at: University of Colorado at Boulder, Boulder, Colorado, USA

Correspondence to: N. Bousseréz (nicolas.bousseréz@colorado.edu)

Abstract. The accuracy of space-based nitrogen dioxide (NO₂) retrievals from solar backscatter radiances critically depends on a priori knowledge of the vertical profiles of NO₂ and aerosol optical properties. This information is used to calculate an air mass factor (AMF), which accounts for atmospheric scattering and is used to convert the measured line-of-sight “slant” columns into vertical columns. In this study we investigate the impact of biomass burning emissions on the AMF in order to quantify NO₂ retrieval errors in the Ozone Monitoring Instrument (OMI) products over these sources. Sensitivity analyses are conducted using the Linearized Discrete Ordinate Radiative Transfer (LIDORT) model. The NO₂ and aerosol profiles are obtained from a 3-D chemistry-transport model (GEOS-Chem), which uses the Fire Locating and Monitoring of Burning Emissions (FLAMBE) daily biomass burning emission inventory. Aircraft in situ data collected during two field campaigns, the Arctic Research of the Composition of the Troposphere from Aircraft and Satellites (ARCTAS) and the Dust and Biomass-burning Experiment (DABEX), are used to evaluate the modeled aerosol optical properties and NO₂ profiles over Canadian boreal fires and western Africa savanna fires, respectively. Over both domains, the effect of biomass burning emissions on the AMF through the modified NO₂ shape factor can be as high as -60 %. A sensitivity analysis also revealed that the effect of aerosol and shape factor perturbations on the AMF is very sensitive to surface reflectance and clouds. As an illustration, the aerosol correction can range from -20 % to +100 % for different surface reflectances, while the shape factor correction varies from -70 % to -20 %. Although previous studies have shown that in clear-sky conditions the effect of aerosols on the AMF was in part implicitly accounted for by the modified cloud parameters, here it is suggested that when clouds are present above a surface layer of scattering aerosols an explicit aerosol correction would be beneficial to the NO₂ retrieval. Finally, a new method that uses slant column information to correct for shape factor-related AMF error over NO_x emission sources is proposed, with possible

application to near-real time OMI retrievals.

25 1 Introduction

Nitrogen oxides ($\text{NO}_x = \text{NO}_2 + \text{NO}$) play a key role in tropospheric chemistry by affecting ozone, atmospheric oxidation, and aerosol formation (Logan, 1983). Biomass burning is a significant source of NO_x , which accounts for 15% of the global emissions (Denman et al., 2007). However this source remains difficult to quantify due to its high spatio-temporal variability (Mebust et al., 2013; 30 Mebust et al., 2011). On the one hand, bottom-up inventories rely on an accurate representation of the different factors controlling NO_x emission from fires, including the type of vegetation, the burning phase and the combustion efficiency (Wiedinmyer et al., 2006; Andrea and Merlet, 2001). This information is generally only available at local scale and extrapolations needed for regional or global estimates are therefore associated with uncertainties. On the other hand, top-down estimates 35 from space-based observations allow to infer regional and global NO_x emissions at relatively high spatial and temporal resolution (Mebust et al., 2013; Mebust et al., 2011; Lamsal et al., 2011; Martin et al., 2003) However, among others, these estimates are affected by errors in the retrieved NO_2 columns (Boersma et al., 2004; Herron-Thorpe et al., 2010). Therefore, quantifying and reducing errors in the NO_2 retrievals is critical to assess and mitigate uncertainties in top-down emission 40 inventories.

Satellite retrievals of NO_2 columns from solar backscatter radiations are based on several steps (Richter and Burrows, 2002; Martin et al., 2002). First, a total slant column is inferred from spectral fitting. A stratospheric contribution is then estimated using either a reference slant column over clean areas or a model simulation in order to derive a tropospheric slant column. The tropospheric 45 slant column is subsequently converted into a vertical column using an air mass factor (AMF). The AMF corrects the measurements for the viewing geometry and the atmospheric scattering effects based on a priori knowledge of the NO_2 profile shapes, surface characteristics (reflectance, pressure) and atmospheric optical properties. It has been shown that the AMF is the largest source of error in NO_2 retrievals (Boersma et al., 2004; Martin et al., 2002). One fundamental issue is related to 50 the fact that the resolution of the input parameters in the AMF calculation is usually much coarser than the satellite pixel area. Recent studies showed that using high-resolution terrain information and NO_2 profile simulations can result in large differences (more than a factor of 2) in the retrieved NO_2 columns compared to products that use a priori data at typical global chemical transport model resolution (Zyrichidou et al., 2013; Heckel et al., 2011; Boersma et al., 2011; Russell et al., 2011; 55 Hains et al., 2010; Zhou et al., 2009). Another approach to tackle the representativeness problem is to use information from the observations themselves, which has been proposed by Lamsal et al. (2008) in the context of top-down estimate of surface NO_2 concentrations. In their study a downscaling technique based on the variability of OMI tropospheric NO_2 columns within a coarse model grid

cell is used to infer NO₂ surface concentration at OMI pixel resolution. Similarly, in this study we
60 will propose a measurement-based correction intended to reduce retrieval errors related to the use of
low resolution NO₂ shape profiles and missing sources in the model.

Besides the difficulty of adequately reproducing NO₂ shape profiles, biomass burning provides
an additional complication by altering the scattering properties of the atmosphere. Previous studies
have investigated the impact of aerosols on the AMF using modeled profiles of aerosol characteristics
65 (Leitão et al., 2010; Martin et al., 2003). Differences in the retrieved NO₂ columns as large as a
factor 2 were obtained when the aerosol effect was not accounted for in the retrieval. An important
finding is that the relative distribution of the aerosol and NO₂ profiles plays a key role in determining
the aerosol effect on the AMF (Leitão et al., 2010; Chen et al., 2009; Fu et al., 2007). Typically,
co-located aerosol and NO₂ layers will tend to increase the AMF, while the presence of an aerosol
70 layer above the boundary layer NO₂ bulk will decrease the AMF (shielding effect). However, it is
still unclear how to account for the aerosol effect, since cloud products used in AMF calculations are
also sensitive to aerosols (Boersma et al., 2011, 2004). Although Boersma et al. (2011) found that
the modified cloud parameters implicitly account for part of the aerosol effect (underestimation of
10-20%), it is unclear to which extent their findings are applicable to retrievals with different aerosol
75 and NO₂ vertical distribution characteristics. Moreover, the case where meteorological clouds and
aerosols are present in the scene has not been studied yet (Leitão et al., 2010).

As a result of all the aforementioned factors, a recent study by Mebust et al. (2011) suggested
that there may be a large negative bias of about 50-100% in the OMI NO₂ retrievals over wildfire.
Further investigation of the properties of NO₂ retrievals over fires is therefore critical. Given the
80 high uncertainty in the prior information used, such study would ideally need to incorporate in situ
observations of aerosols and NO₂ profiles over different type of fires.

The Arctic Research of the Composition of the Troposphere from Aircraft and Satellites (ARC-
TAS) and The Dust And Biomass EXperiment (DABEX) experiments provide extensive aircraft in
situ measurements of NO₂ concentrations and aerosol optical properties over boreal and savanna
85 fires, respectively. ARCTAS-B took place in June–July 2008 with a major emphasis on boreal forest
fire influences over Canada (Parrington et al., 2013; Corr et al., 2012; Jacob et al., 2010). DABEX,
part of the African Monsoon Multidisciplinary Analysis (AMMA) experiment, took place in Jan-
uary 2006 over west Africa (Johnson et al., 2008a; Capes et al., 2008; Redelsperger et al., 2006).
These two campaigns provide an unprecedented dataset to evaluate modeled aerosol and NO₂ pro-
90 files that are used in the AMF calculation over different biomass burning regions. To our knowledge,
a comprehensive analysis of NO₂ retrievals over biomass burning supported by detailed aerosol and
NO₂ in situ measurements has not been conducted yet.

In this study, the impact of biomass burning emissions on the AMF is assessed using the the
Linearized Discrete Ordinate Radiative Transfer (LIDORT) model (Spurr et al., 2001; Spurr, 2002)
95 combined with aerosol and NO₂ profiles from a GEOS-Chem 3-D chemistry transport model (CTM)

simulation with daily-resolved fire emissions from Fire Locating and Monitoring of Burning Emissions (FLAMBE) (Reid et al., 2009). In Section 2, the theoretical basis for the AMF algorithm is introduced. In Section 3, a detailed description of the ARCTAS-B and DABEX experiments is provided. In Section 4, the modeled aerosol optical properties and NO₂ profile shapes are evaluated against the ARCTAS and DABEX observations. In Sections 5 to 8, the sensitivity of the AMF to biomass burning emissions and its dependence to several retrieval parameters is investigated. Finally, in Section 9, an approach based on slant column measurement information to reduce AMF errors associated with NO₂ shape factor uncertainties is proposed.

2 AMF calculation

The tropospheric AMF is defined as the ratio of the tropospheric slant column, which is the total tropospheric amount of trace gas along an average backscattered path observed by a satellite instrument, to the tropospheric vertical column of this trace gas. Following Palmer et al. (2001), the tropospheric AMF can be expressed as

$$\text{AMF} = \text{AMF}_G \int_0^1 \omega(\sigma) S(\sigma) d\sigma \quad (1)$$

In this equation AMF_G is the geometric AMF accounting for the satellite viewing geometry. The term σ represents the sigma vertical coordinate of the model, related to the pressure P by $P = \sigma(P_S - P_T) + P_T$, where P_S and P_T are the pressure at the surface and the top of the troposphere, respectively. $S(\sigma)$ is the *shape factor*, a dimensionless normalized NO₂ vertical profile, and $\omega(\sigma)$ are the scattering weights describing the sensitivity of the backscattered spectrum to the abundance of NO₂ at each σ -level.

The AMF formulation used takes into account cloud-contaminated pixels following the independent pixel approximation, as described in Martin et al. (2002). The cloud fraction and cloud pressure are retrieved from OMI using the O₂-O₂ algorithm (Acarreta et al., 2004). Surface reflectivity was obtained from a climatology from OMI at 440 nm (Kleipool et al., 2008). Scattering weights are calculated using the Linearized Discrete Ordinate Radiative Transfer (LIDORT) model (Spurr et al., 2001; Spurr, 2002). The NO₂ shape factors and aerosol optical characteristics are obtained from a GEOS-Chem simulation described in Appendix A.

3 Observational dataset

3.1 ARCTAS-B campaign

The summer ARCTAS-B campaign took place in late June and early July 2008 (Jacob et al., 2010). The primary goal of this experiment was to better understand the factors driving current changes in Arctic atmospheric composition and climate.

The campaign included the DC-8 research aircraft to measure chemical and radiative properties of the atmosphere. From 26 June to 14 July 2008, the aircraft was based in Cold Lake, Canada (54° N, 110° W), where it sampled many fresh and aged biomass burning plumes at a wide range of altitudes (Alvarado et al., 2010). Figure 1 shows the DC-8 aircraft flight paths during that experiment. The DC-8 included highly sensitive high-frequency (1–10 s) measurements of key ozone precursors (NO_y, HO_x, PAN, HCHO) as well as aerosol optical and physical properties. Measurement characteristics for the species considered in this study are summarized Table 1. For a more detailed description of the chemical and optical properties of biomass burning plumes sampled during ARCTAS-B the reader is referred to Singh et al. (2010) and Alvarado et al. (2010).

3.2 DABEX campaign

The African Monsoon Multidisciplinary Analysis (AMMA) is a major international experiment designed to improve our understanding of the west African monsoon (Redelsperger et al., 2006). The Dust And Biomass burning EXperiment (DABEX) was part of the Special Observing Period (SOP) dry season (January–February 2006). It was carried out over western Africa by the UK Met Office, which used the FAAM BAe-146 aircraft to perform high-quality in situ measurements of the chemical, optical and physical properties of biomass burning and dust aerosols over western Africa. Figure 1 shows the FAAM BAe-146 flight tracks during DABEX. The area sampled covered a narrow domain spanning from western Niger, where mineral dust is predominant, to center Benin, where savanna fires occur,

Physical and optical properties of dust and biomass burning aerosols during DABEX were analyzed in detail in several studies (Johnson et al., 2008a,b; Osborne et al., 2008; Capes et al., 2008). Analysis of fresh biomass burning aerosols was especially challenging due to frequent mixing with mineral dust near the surface. Nevertheless, results show similar aerosol characteristics than previously found during the SAFARI-2000 campaign over southern Africa (Haywood et al., 2003).

Table 2 summarizes the measurement characteristics for the data considered in this study. To complete our model evaluation, we also used aerosol optical depth (AOD) and single scattering albedo (SSA) surface in situ data from the Aerosol Robotic Network (AERONET) network, which consist of sun photometer measurements (Dubovik et al., 2002). Figure 1 shows the locations of the AERONET stations considered for this study.

4 Model evaluation

The GEOS-Chem 3-D chemistry transport model described in Appendix A is a central tool in our AMF analysis, since it provides the aerosol and NO₂ profiles used in the radiative transfer calculation. The GEOS-Chem simulation is performed at a 2°, latitude × 2.5° horizontal grid resolution and uses a global daily biomass burning emission inventory. Aerosol optical properties in GEOS-

Chem are simulated following Martin et al. (2003). Here the modeled aerosol optical properties and NO₂ profiles were evaluated against aircraft in situ measurements from the DABEX and ARCTAS campaigns. For this purpose, model outputs were interpolated along the flight tracks and filtered to
165 retain only observations influenced by biomass burning emissions.

For ARCTAS, measurements impacted by biomass burning emissions were identified by enhancements in HCN and CO concentrations greater than 20% of the regional background.

For DABEX, measurements influenced by biomass burning were defined according to Johnson et al. (2008b), who derived the following criteria:

- 170
- scattering at 550 nm (green) > 30.10⁻⁶ m
 - Angström exponent > 1

A model sensitivity simulation was performed to ensure that the selected observations were also associated with biomass burning influences in the model. Mean modeled and observed profiles were subsequently derived by vertically binning the data over the entire ARCTAS (150–80° W; 49–70° N) and DABEX (2° W–8° E; 8–20° N) domains.
175

Figure 2 shows the observed and simulated shape factor, aerosol extinction coefficient (440 nm) and SSA (440 nm) mean profiles during ARCTAS. There is an overall good agreement between the model and the measurements. The NO₂ shape factor shows a sharp enhancement near the surface due to fire emissions. Model analyses (not shown) suggest that the gradient observed at the top of the troposphere and not seen in the model is due to an underestimation of lightning NO_x emissions.
180 Aerosol extinction coefficients also increase in the boundary layer as a result of biomass burning emissions. The shape and magnitude of the extinction is similar in the model and the measurements. The mean SSA profile is also reasonably well reproduced by the model, with relatively homogeneous values of 0.90–0.95. These observations are consistent with SSA values derived by Reid et al. (2005)
185 over boreal fires using AERONET measurements.

Figure 2 shows the profiles of the shape factor, aerosol extinction coefficient (440 nm) and aerosol scattering coefficient (440 nm) from GEOS-Chem and the FAAM BAe-146 measurements during DABEX. Since aerosol absorption measurements were available only at 565 nm, the observed extinction at 565 nm has been scaled to 440 nm by applying the ratio between the scattering coefficients
190 at 440 nm and 565 nm. In order to conserve original measurements in the comparison, here the choice has been made to show the scattering coefficient at 440 nm instead of the SSA. The modeled and observed shape factors show a significant increase near the surface, similar to the one observed over boreal fires. Aerosol extinction and scattering coefficient profile shapes are well reproduced by GEOS-Chem. The model underestimation near the surface may be attributed to representativeness
195 errors given the coarse resolution used. Note that the poor sampling of the boundary layer during DABEX limits confidence in the results near the surface. Aerosol extinction coefficients measured over savanna fires (~0.4–0.8 km⁻¹) are significantly greater than those observed over boreal fires

during ARCTAS ($\sim 0.1\text{--}0.2\text{ km}^{-1}$). Again, the boundary layer observations during DABEX are representative of specific fire events rather than average characteristics. Table 3 contains the AOD and SSA columns for GEOS-Chem and the AERONET measurements at several stations in western Africa. The modeled SSA agrees with observations within 0.02 in average, and the modeled AOD within 23 %.

In conclusion, the evaluation of the GEOS-Chem NO_2 profiles and aerosol optical properties over boreal and savanna fires shows that the model represents reasonably well their main characteristics. In the following, aerosol and NO_2 profiles simulated by GEOS-Chem are used to calculate the AMF and to analyze its sensitivity to biomass burning emissions.

5 Impact of biomass burning emissions on the AMF

Generally the high spatial and temporal variability of fire emissions is not fully resolved in CTMs. This is in part due to representativeness errors owing to the coarse resolution of the model simulations as well as to incomplete knowledge of the different factors influencing fire emissions, such as the vegetation type and the combustion efficiency. Assuming the aerosol effect is at least partially accounted for by the cloud correction, only the impact of biomass burning on the NO_2 shape factor is considered here (the aerosol effects are not explicitly account for in the AMF). A shape factor correction associated with fire emissions can be defined as the ratio between an AMF that includes biomass burning emissions and an AMF that does not include these emissions:

$$\text{AMF}_{\text{cor}} = \frac{\text{AMF}_{\text{bb}}}{\text{AMF}_{\text{nobb}}} \quad (2)$$

where subscripts on the right hand side specify if biomass burning emissions are included (bb) or not (nobb) in the AMF calculation.

Figure 3 shows the mean shape factor correction over boreal and savanna fires during ARCTAS and DABEX, respectively. Only OMI scenes with cloud fraction $< 5\%$ have been considered here in order to limit the interference of clouds in the analysis while retaining a statistically significant number of data. The AMF correction ranges from -60 to 0% . Fire emissions reduce the AMF by increasing the NO_2 shape factor near the surface (and decreasing it above) where measurement sensitivity is minimum. These results show that NO_2 retrievals over fires can underestimate NO_2 tropospheric columns by a factor 2 when some of these sources are missing in the model. This scenario will generally correspond to wildfire events, which are by nature unpredictable and whose emissions cannot be accounted for in real-time in the retrievals. Note that the AMF correction presented here does not take into account representativeness errors due to the coarse model resolution. This problem will be addressed in Section 9.

Also, although here it is assumed that the aerosol effect is implicitly accounted for by the cloud correction algorithm, this assumption has been questioned in a recent study by Leitão et al. (2010) in the case of cloudy scenes. A better understanding of the effect of aerosols on the AMF can help

investigating this issue further. This effect needs to be characterized for different retrieval parameters (e.g. SSA, surface reflectance). Similarly, the impact of the modified NO₂ shape factor on the AMF is modulated by changes in these parameters. s

In the next two sections we study in detail the sensitivity of the AMF to aerosol and NO₂ shape factor perturbations for a case representative of the conditions found over savanna fires during the DABEX campaign.

6 Aerosol correction factor sensitivity analysis

240 In this section, we assess the influence of aerosols on the AMF and its dependence to aerosol characteristics (optical properties, profile shape) as well as key retrieval parameters (satellite viewing geometry, surface reflectance, clouds). A sensitivity analysis is conducted using a reference profile for aerosols and NO₂ from a GEOS-Chem simulation during DABEX. The reference solar zenith angle (SZA), SSA and surface reflectance are 40°, 0.91, and 0.03 respectively. In the sensitivity 245 experiment, each parameter varies while others are kept constant. Since the model horizontal resolution (2° × 2.5°) is much coarser than OMI's, and in order to minimize the representativeness error above biomass burning sources, the grid cell associated with highest emissions during the DABEX period has been selected. Figure 4 shows the corresponding simulated NO₂ and aerosol profiles at OMI overpass time (13:30 PM – local time). The presence of an elevated aerosol layer is consistent 250 with previous observations and analyses over African biomass burning regions (Jury and Whitehall (2010); Anderson et al. 1996; Johnson et al. (2008)). During DABEX, this pattern has been shown to be due to the uplift of biomass burning aerosols by the Harmattan front (Haywood et al., 2008).

The aerosol correction factor is defined as the ratio between an AMF that includes aerosol effects and an AMF that does not include them. The sensitivity of the aerosol correction factor to aerosol 255 profile shape has been evaluated by comparing the correction with and without the elevated aerosol layer, as represented Fig. 4. As a result of the shielding effect, the aerosol correction factor decreases from +20 to -30 % in the presence of the elevated aerosol layer.

Figure 5 shows the influence of SSA, SZA and surface reflectance on the aerosol correction factor for the two types of profile considered. For each of these parameters, the sensitivity of the aerosol 260 correction factor is similar whether or not the elevated aerosol layer is included. The AMF being a vertical integration of the scattering coefficients weighted by the NO₂ shape factor, its sensitivity is driven by optical properties near the surface where the NO₂ shape factor peaks, which explains the similarities observed.

The aerosol correction factor is very sensitive to surface reflectance. We observe an exponential 265 decay, which reflects the competing effects of the measurement sensitivity increase due to scattering above the aerosol layer and the shielding effect below it. We see that the relative impact of the shielding effect increases quickly with surface reflectance with an asymptotic limit for surface

reflectance > 0.1 . For surface only aerosols, the correction varies from +100 % for very low surface reflectance to -20 % for surface reflectance > 0.1 .

270 A linear increase of the aerosol correction factor with SSA is observed, while the viewing geometry (SZA) has negligible impact on the correction, which is consistent with findings by Leitão et al. (2010) over urban areas.

The impact of emission intensity on the aerosol correction factor has been assessed by re-scaling the aerosol and NO_2 concentrations within a 0–1 km surface layer. Figure 5 d) shows that the effect
275 of aerosols on the AMF is almost insensitive to emission intensity. This reflects the balance between the AMF increase caused by aerosol scattering effects and the AMF decrease due to NO_2 shape factor enhancements at the surface. A direct consequence is that the aerosol correction factor will be only weakly impacted by emission representativeness errors within one model grid cell as long as the aerosol/ NO_2 emission factors are homogeneous inside that domain.

280 The presence of clouds above the aerosol layer can modify the aerosol correction factor through its shielding effect. Figure 6 shows the aerosol correction factor as a function of cloud fraction for different AODs, and for the two aerosol profiles considered in Fig. 4. Here the cloud top pressure was set to 460 hPa, which corresponds to clouds above the elevated aerosol layer. For any AOD value, the aerosol correction factor increases linearly with cloud fraction. This reflects the higher relative
285 impact of aerosol scattering on the AMF for higher shielding effects, due to the aerosol correction being a ratio of smaller AMFs. Note that increasing the optical thickness of the elevated aerosol layer does not modify the sensitivity of the aerosol correction factor to cloud fraction. This is expected since an elevated aerosol layer will essentially play the same role as an increase in cloud fraction in the retrieval algorithm. However, in the case where NO_2 and aerosols are co-located near the
290 surface, the aerosol correction factor sensitivity to cloud radiance fraction increases with AOD. As a result, for an AODs > 1 , which is commonly measured over biomass burning events (Gogoi et al., 2013), we see from Fig. 6 that the aerosol correction can vary from +20 % to +100 % between clear-sky and cloudy (cloud fraction of 20 %) conditions. As discussed in Boersma et al. (2011, 2004), it is important to realize that in real retrieval conditions aerosols will impact the retrieved clouds
295 parameters used in the AMF calculation. This important aspect is discussed in the next section.

7 Do clouds implicitly account for aerosol effects?

Since aerosols impact the retrieved cloud parameters in the UV-Vis, correcting AMFs for aerosols cannot be decoupled from correcting cloud retrieval schemes for aerosols. In Boersma et al. (2011, 2004), it is shown that the effect of aerosols on the AMF is partly accounted for through the modified
300 cloud parameters for clear-sky scenes and exponentially decreasing shape profiles for aerosols and NO_2 . However, as Leitão et al. (2010) explained, if clouds are present above a surface layer of scattering aerosols, the retrieved cloud fraction will be enhanced, while the cloud pressure will

remain unchanged. Therefore, instead of increasing the AMF and implicitly correcting for aerosol effects, the modified cloud fraction will in fact decrease the AMF. In this case, explicitly accounting
305 for the aerosol scattering effect would counterbalance the additional shielding effect from clouds and may therefore improve the retrieval. This is illustrated by the following relationships, valid for cloudy retrievals including a surface layer of scattering aerosols:

$$AMF^{\delta cloud} < AMF_{aerosol}^{\delta cloud} \leq AMF_{aerosol} \quad (3)$$

where ‘aerosol’ indicates that an explicit aerosol correction is used, and $\delta cloud$ represents the perturbation of cloud fraction by aerosols. Here we see that the AMF using an explicit aerosol correction
310 factor ($AMF_{aerosol}^{\delta cloud}$) yields a better approximation to the true AMF ($AMF_{aerosol}$). The fact that it is theoretically possible to reproduce the true AMF (weak inequality) follows from our previous result that an increase in cloud fraction induces an increase in the aerosol correction factor. Therefore, this suggests that in the presence of clouds and surface scattering aerosols, the aerosol effects should be
315 explicitly accounted for in the AMF calculation. On the other hand, as explained in Leitão et al. (2010), if the surface aerosols are very absorbing, the retrieved cloud fraction will be reduced, which cannot compensate for the shielding effect of aerosol absorption.

8 Shape factor correction sensitivity analysis

The impact of biomass burning emissions on the AMF through the modified NO_2 shape factors is
320 also altered by changes in other retrieval parameters. Figure 7 shows the sensitivity of the shape factor correction to cloud fraction and surface reflectance. The shape factor correction decreases almost linearly with cloud fraction. The shape factor-related AMF errors varies from -60 % to -80 % between clear-sky conditions and a cloud fraction of 30 %.

Similarly to the aerosol correction factor, the shape factor correction is highly sensitive to surface
325 reflectance at low values (0-0.1). As an illustration, for the surface reflectance associated with our reference case over west African fires (0.03), the AMF error associated with missing fire sources can be as high as 60 %, but only %20 for a surface reflectance of 0.3. This highlights the need for high spatial resolution surface albedo climatology in the AMF calculation, as has been recently implemented in an improved OMI NO_2 product by Boersma et al. (2011).

330 9 Measurement-based shape factor correction

It has been recently shown that uncertainties in the simulated NO_2 shape factors and in surface albedo input data are the dominant sources of error in the AMF (Heckel et al., 2011). Of concern is that current operational OMI NO_2 retrievals cannot fully represent the true spatial and temporal variation of NO_2 profiles needed for accurate retrievals over fast-changing sources (e.g. biomass
335 burning). For instance, the NASA standard OMI NO_2 product uses geographically gridded yearly

average NO₂ profiles from a GEOS-Chem simulation (Martin et al., 2003). Here we investigate a method to infer shape factor corrections using measurement information. As explained in Sect. 2, measurement information is contained in the slant columns. Over high NO_x sources like fires, most of the NO₂ column will be concentrated in the boundary layer (Lamsal et al., 2008; Bucsele et al., 340 2008). Local variability of the slant columns will therefore be primarily affected by variability of the lower part of the NO₂ profile.

Here we use this property to establish a relationship between the shape factor correction and the associated slant column perturbation, defined as the relative increase of the slant column with respect to a case without biomass burning emissions. Slant columns and shape factor corrections 345 are computed using a pseudo-retrieval experiment, in which OMI NO₂ averaging kernels are applied to the GEOS-Chem NO₂ profiles (Eskes et al., 2003). Two GEOS-Chem simulations, one using daily biomass burning emissions (BB_{sim}), and one with biomass burning emissions turned off (NOBB_{sim}) are used to generate three types of pseudo NO₂ retrievals:

- *A*, of BB_{sim} using NO₂ shape factors from NOBB_{sim};
- 350 - *B*, of NOBB_{sim} using NO₂ shape factors from NOBB_{sim};
- *C*, of BB_{sim} using NO₂ shape factors from BB_{sim}.

Note that using a perfect shape factor in *B* and *C* (the one corresponding to the column retrieved) results in *B* and *C* being the actual GEOS-Chem columns.

We further define:

- 355 - $\Delta\text{NO}_2 = \frac{A-B}{B}$, the relative NO₂ column increase compared to the case without biomass burning;
- NO₂ correction factor = $\frac{C}{A}$.

Since the same AMF is used in *A* and *B* (AMF_{*A*}=AMF_{*B*}), the dependence of ΔNO_2 to measurement information can be made explicit by rewriting:

$$360 \quad \Delta\text{NO}_2 = \frac{\frac{\text{Slt}_A}{\text{AMF}_A} - \frac{\text{Slt}_B}{\text{AMF}_B}}{\frac{\text{Slt}_B}{\text{AMF}_B}} \quad (4)$$

$$= \frac{\text{Slt}_A - \text{Slt}_B}{\text{Slt}_B}$$

where ‘Slt’ represents the slant column. Figure 8 shows the relationship between ΔNO_2 and the NO₂ correction factor over western Africa fires during DABEX. The correction factor increases with ΔNO_2 with a “saturation effect” for $\Delta\text{NO}_2 > 4$, where the NO₂ correction is almost constant (=3). 365 Further increasing NO_x emissions above this threshold does not change the shape factor since almost

the totality of the NO_2 column is already concentrated in the boundary layer. The relationship between the NO_2 correction factor and ΔNO_2 can be well approximated by the following logarithmic fit:

$$\text{NO}_2 \text{ correction factor} = \log(3.4 \Delta\text{NO}_2 + 2.2). \quad (5)$$

370 The above formula can be applied to real retrievals by replacing the pseudo slant columns Sl_A in Eq. 4 by the retrieved NO_2 slant column, and assuming the pseudo slant column Sl_B is a good approximation of what would be the retrieved slant column without the fire source. The standard deviations of the NO_2 correction in Fig. 8 can be interpreted as the errors associated with the logarithmic fit approximation (Eq. 5). Although large standard deviations are observed, one sees that
375 they are all significantly smaller than the mean NO_2 correction itself. Using this measurement-based correction should therefore reduce NO_2 retrieval errors over fires.

Although this correction has been derived for retrievals over western Africa fire sources, it could easily be extended to other regions and sources. In an operational near-real time retrieval setting, ΔNO_2 in eq. 5 can be obtained using a “clean” NO_2 profile to derive Sl_B (reference “clean” slant
380 column) and A . For instance, the reference NO_2 profile can be taken from a model simulation without NO_x emissions. Note that the availability of the retrieval averaging kernels is necessary in order to apply the proposed methodology.

This measurement-based correction is intended to reduce uncertainties related to both representativeness errors and misrepresentation of the location and time of NO_x emissions in model simula-
385 tions. Due to the lack of aircraft measurements in the boundary layer during DABEX, our approach cannot be rigorously evaluated using in situ-derived NO_2 columns. A study using in situ data from previous aircraft campaigns (e.g. INTEX-A, INTEX-B, PAVE) (see also more recently Oetjen et al. (2013)) as well as from ground-based measurements of NO_2 columns (Ma et al., 2013; Rivera et al., 2013; Irie et al., 2012) would allow to properly evaluate the robustness of the above formula for
390 different retrieval conditions as well as to better characterize errors.

10 Conclusions

In this study, the sensitivity of the air mass factor (AMF) to biomass burning emissions is analyzed in order to better characterize and understand NO_2 retrieval uncertainties over fire areas. The radiative transfer model (LIDORT) used to calculate the AMF can treat both aerosols and clouds effects.
395 Aerosols and NO_2 profiles are obtained from a CTM simulation (GEOS-Chem) which uses daily-resolved biomass burning emissions (FLAMBE). The simulated aerosol optical properties and NO_2 profiles were evaluated over Canadian and western Africa fires using aircraft in situ measurements from the ARCTAS-B 2008 and DABEX 2006 campaigns, respectively.

In clear-sky conditions (cloud fraction $<5\%$), the effect of biomass burning emissions on the
400 AMF through the modified NO_2 shape factor ranges from -60% to 0% over both boreal and sa-

vanna fires. These values provide an estimate of the AMF errors associated with NO₂ shape factor uncertainties due to missing fire sources in the model, but representativeness errors associated with low resolution NO₂ shape profiles can further enhance these errors. The influence of several retrieval parameters (surface reflectance, clouds, viewing geometry) on the AMF sensitivity to aerosols and shape factors was also analyzed. Both aerosol and shape factor effects are very sensitive to surface reflectance. As an illustration, the aerosol correction can range from -20 % to +100 % for different surface reflectances, while the shape factor correction varies from -70 % to -20 %. Using highly spatially resolved surface reflectance data is therefore critical to mitigate NO₂ retrieval errors over biomass burning areas. It was found that the intensity of fire emissions does not significantly impact the effect of aerosol for a given NO₂/aerosols emission ratio. This suggests that emissions-related representativeness errors may be weak when modeling the aerosol effects. It was found that the impact of biomass burning emissions on the AMF is also very sensitive to clouds. The aerosol and shape factor corrections can vary from +20 % to +100 % and -60 % to -80 %, respectively, when a cloud fraction of 20 % is added to the scene.

Since the OMI clouds retrieval is sensitive to aerosols, previous studies suggested that the aerosol effect on the AMF was implicitly accounted for through the modified cloud parameters. A previous analysis by Leitão et al. (2010) and results from our sensitivity experiment suggest that when clouds are present above a scattering aerosols layer, taking explicitly aerosol effects into account should improve the AMF calculation. More investigations based on sensitivity experiments simulating the effect of aerosols on the cloud retrieval would be necessary to better understand in what cases an explicit aerosol correction would be beneficial to the retrieval.

Finally, a new method has been proposed to reduce NO₂ retrieval errors associated with misrepresentations of the NO₂ shape profile in the AMF calculation. The approach is based on the local sensitivity of the slant column to NO₂ sources. Using a pseudo-retrieval analysis, a relationship between the AMF shape factor correction and the associated slant column perturbation was established. Although this measurement-based correction has been derived over African fires, it could be extended to any type of NO_x source. In practice it requires only the retrieval averaging kernel information as well as a “clean” NO₂ reference profile, typically obtained from a model simulation. Future studies using in situ-derived NO₂ columns over urban and biomass burning regions would allow a proper evaluation of the method and will help assess its relevance for existing operational OMI NO₂ retrievals.

Appendix A GEOS-Chem simulations

GEOS-Chem is a global 3-D chemical transport model driven by assimilated meteorological observations from the Goddard Earth Observing System (GEOS) of the NASA Global Modeling and Assimilation Office (GMAO) (www.geos-chem.org; Bey et al., 2001). We use the GEOS-5 meteorolo-

logical data regridded to 2° , latitude $\times 2.5^\circ$, longitude, with 47 vertical layers. For both the DABEX and ARCTAS-B period we use the NRT-ARCTAS GEOS-Chem simulation, which was originally developed in support of the ARCTAS mission and is based on GEOS-Chem v8-01-01 with minor modifications (Mao et al., 2010). The simulation includes ozone-NO_x-HO_x-VOC-aerosol chemistry
440 as described in Park et al. (2005).

A daily biomass burning emission inventory at $1^\circ \times 1^\circ$ resolution obtained from Fire Locating and Monitoring of Burning Emissions (FLAMBE) (Reid et al., 2009) is used to capture the high spatial and temporal variability of fire emissions. The FLAMBE product is constrained by Geostationary Operational Environmental Satellite (GOES) and Moderate Resolution Imaging Spectrometer
445 (MODIS) fires count data and provides daily global smoke and carbon emissions. Emissions for black carbon and organic carbon species in GEOS-Chem are obtained by applying emission factors to the FLAMBE smoke emissions, while emissions for other species, including NO_x, are derived by applying emission factors to the FLAMBE carbon emissions. Emission factors are those proposed by Andreae and Merlet (2001). Further information about the biomass burning emissions in the
450 model can be found in Fisher et al. (2010).

Dust aerosol concentrations can be significant over west Africa due to transport from the Sahara desert. The mineral dust module in GEOS-Chem simulates the mobilization of dust from the Earth's surface, gravitational settling, and wet and dry deposition as described in Fairlie et al. (2007).

For our ARCTAS simulation, a 70 % decrease of carbon emissions and a 60 % decrease of smoke
455 emissions in the FLAMBE inventory, as well as the use of an extra-tropical forest fires NO_x emission factor of 0.42 g NO/kg DM (Alvarado et al., 2010) were required in order to match the aircraft in situ observations.

Acknowledgements. This work was supported by the Canadian Foundation for Climate and Atmospheric Sciences. Nicolas Bousserez would also like to acknowledge support from NASA grant NNX09AN77G.

460 References

- Acarreta, J., De Haan, J., and Stammes, P.: Cloud pressure retrieval using the O₂-O₂ absorption band at 477 nm, *J. Geophys. Res.-Atmos.*, 109, D05204, doi:10.1029/2003JD003915, 2004.
- Anderson, T.L., Ogren, J.A.: Determining aerosol radiative properties using the TSI 3563 integrating nephelometer, *Aerosol Science and Technology*, Vol 29 , (1), 57-69, 1998
- 465 Andreae, M.O. and Merlet, P.: Emission of trace gases and aerosols from biomass burning. *Global Biogeochem. Cycles* 15, 955-966, 2001.
- Alvarado, M. J., Logan, J. A., Mao, J., Apel, E., Riemer, D., Blake, D., Cohen, R. C., Min, K.-E., Perring, A. E., Browne, E. C., Wooldridge, P. J., Diskin, G. S., Sachse, G. W., Fuelberg, H., Sessions, W. R., Harrigan, D. L., Huey, G., Liao, J., Case-Hanks, A., Jimenez, J. L., Cubison, M. J., Vay, S. A., Weinheimer, A. J., Knapp, D. J., Montzka, D. D., Flocke, F. M., Pollack, I. B., Wennberg, P. O., Kurten, A., Crounse, J., St. Clair, J. M., Wisthaler, A., Mikoviny, T., Yantosca, R. M., Carouge, C. C., and Le Sager, P.: Nitrogen oxides and PAN in plumes from boreal fires during ARCTAS-B and their impact on ozone: an integrated analysis of aircraft and satellite observations, *Atmos. Chem. Phys.*, 10, 9739–9760, doi:10.5194/acp-10-9739-2010, 2010.
- 470 Anderson, B. E., W. B. Grant, G. L. Gregory, E. V. Browell, J. E. Collins Jr., G. W. Sachse, D. R. Bagwell, C. H. Hudgins, D. R. Blake, and N. J. Blake: Aerosols from biomass burning over the tropical South Atlantic region: Distributions and impacts, *J. Geophys. Res.*, 101(D19), 2411724137, doi:10.1029/96JD00717, 1996
- Bey, I., Jacob, D., Yantosca, R., Logan, J., Field, B., Fiore, A., Li, Q., Liu, H., Mickley, L., and Schultz, M.: Global modeling of tropospheric chemistry with assimilated meteorology: Model description and evaluation, *J. Geophys. Res.-Atmos.*, 106, 23073–23095, doi:10.1029/2001JD000807, 2001.
- 480 Boersma, K. F., Eskes, H., and Brinksma, E.: Error analysis for tropospheric NO₂ retrieval from space, *J. Geophys. Res.-Atmos.*, 109, D04311, doi:10.1029/2003JD003962, 2004.
- Boersma, K. F., Eskes, H. J., Veefkind, J. P., Brinksma, E. J., van der A, R. J., Sneep, M., van den Oord, G. H. J., Levelt, P. F., Stammes, P., Gleason, J. F., and Bucsela, E. J.: Near-real time retrieval of tropospheric NO₂ from OMI, *Atmos. Chem. Phys.*, 7, 2103–2118, doi:10.5194/acp-7-2103-2007, 2007.
- 485 Boersma, K. F., Eskes, H. J., Dirksen, R. J., van der A, R. J., Veefkind, J. P., Stammes, P., Huijnen, V., Kleipool, Q. L., Sneep, M., Claas, J., Leitão, J., Richter, A., Zhou, Y., and Brunner, D.: An improved tropospheric NO₂ column retrieval algorithm for the Ozone Monitoring Instrument, *Atmos. Meas. Tech.*, 4, 1905–1928, doi:10.5194/amt-4-1905-2011, 2011.
- Bucsela, E. J., et al.: Comparison of tropospheric NO₂ from in situ aircraft measurements with near-real-time and standard product data from OMI, *J. Geophys. Res.*, 113, D16S31, doi:10.1029/2007JD008838, 2008
- 490 Capes, G., Johnson, B., McFiggans, G., Williams, P. I., Haywood, J., and Coe, H.: Aging of biomass burning aerosols over West Africa: Aircraft measurements of chemical composition, microphysical properties, and emission ratios, *J. Geophys. Res.-Atmos.*, 113, D00C15, doi:10.1029/2008JD009845, 2008.
- Chen, D., Zhou, B., Beirle, S., Chen, L. M., and Wagner, T.: Tropospheric NO₂ column densities deduced from zenith-sky DOAS measurements in Shanghai, China, and their application to satellite validation, *Atmos. Chem. Phys.*, 9, 36413662, 2009
- 495 Cleary, PA, Wooldridge, PJ, Cohen, RC: Laser-induced fluorescence detection of atmospheric NO₂ with a commercial diode laser and a supersonic expansion, *Applied Optics*, Vol. 41, (33), 6950-6956, 2002
- Corr, C. A., Hall, S. R., Ullmann, K., Anderson, B. E., Beyersdorf, A. J., Thornhill, K. L., Cubison, M.

- 500 J., Jimenez, J. L., Wisthaler, A., and Dibb, J. E.: Spectral absorption of biomass burning aerosol determined from retrieved single scattering albedo during ARCTAS, *Atmos. Chem. Phys.*, 12, 10505-10518, doi:10.5194/acp-12-10505-2012, 2012.
- Dubovik, O., Holben, B., Eck, T., Smirnov, A., Kaufman, Y., King, M., Tanre, D., and Slutsker, I.: Variability of absorption and optical properties of key aerosol types observed in worldwide locations, *J. Atmos. Sci.*, 59, 590–608, doi:10.1175/1520-0469(2002)059, 2002.
- 505 Eskes, H. J. and Boersma, K. F.: Averaging kernels for DOAS total-column satellite retrievals, *Atmos. Chem. Phys.*, 3, 1285-1291, doi:10.5194/acp-3-1285-2003, 2003.
- Fairlie, T. D., Jacob, D. J., and Park, R. J.: The impact of transpacific transport of mineral dust in the United States, *Atmos. Environ.*, 41, 1251–1266, doi:10.1016/j.atmosenv.2006.09.048, 2007.
- 510 Fisher, J. A., Jacob, D. J., Purdy, M. T., Kopacz, M., Le Sager, P., Carouge, C., Holmes, C. D., Yantosca, R. M., Batchelor, R. L., Strong, K., Diskin, G. S., Fuelberg, H. E., Holloway, J. S., Hyer, E. J., McMillan, W. W., Warner, J., Streets, D. G., Zhang, Q., Wang, Y., and Wu, S.: Source attribution and interannual variability of Arctic pollution in spring constrained by aircraft (ARCTAS, ARCPAC) and satellite (AIRS) observations of carbon monoxide, *Atmos. Chem. Phys.*, 10, 977–996, doi:10.5194/acp-10-977-2010, 2010.
- 515 Fu, T.-M., Jacob, D. J., Palmer, P. I., Chance, K., Wang, Y. X., Barletta, B., Blake, D. R., Stanton, J. C., and Pilling, M. J.: Space-based formaldehyde measurements as constraints on volatile organic compound emissions in east and south Asia and implications for ozone, *J. Geophys. Res.*, 112, D06312, doi:10.1029/2006JD007853, 2007
- Gogoi M.M., S. Suresh Babu, K. Krishna Moorthy, M.R. Manoj, Jai Prakash Chaubey: Absorption characteristics of aerosols over the northwestern region of India: Distinct seasonal signatures of biomass burning aerosols and mineral dust, *Atmospheric Environment*, Volume 73, July 2013, Pages 92-102, 2013
- 520 Hains, J. C., Boersma, K. F., Kroon, M., Dirksen, R. J., Cohen, R. C., Perring, A. E., Bucsel, E., Volten, H., Swart, D. P. J., Richter, A., Wittrock, F., Schoenhardt, A., Wagner, T., Ibrahim, O. W., van Roozendaal, M., Pinardi, G., Gleason, J. F., Veefkind, J. P., and Levelt, P.: Testing and improving OMI DOMINO tropospheric NO₂ using observations from the DANDELIONS and INTEX-B validation campaigns, *J. Geophys. Res.-Atmos.*, 115, D05301, doi:10.1029/2009JD012399, 2010.
- Haywood, J. M., Pelon, J., Formenti, P., Bharmal, N., Brooks, M., Capes, G., Chazette, P., Chou, C., Christopher, S., Coe, H., Cuesta, J., Derimian, Y., Desboeufs, K., Greed, G., Harrison, M., Heese, B., Highwood, E. J., Johnson, B., Mallet, M., Marticorena, B., Marsham, J., Milton, S., Myhre, G., Osborne, S. R., Parker, D. J., Rajot, J., Schulz, M., Slingo, A., Tanre, D., and Tulet, P.: Overview of the Dust and Biomass-burning Experiment and African Monsoon Multidisciplinary Analysis Special Observing Period-0, *J. Geophys. Res.-Atmos.*, 113, D00C17, doi:10.1029/2008JD010077, 2008.
- 530 Haywood, J. M., S. R. Osborne, P. N. Francis, A. Keil, P. Formenti, M. O. Andreae, and P. H. Kaye: The mean physical and optical properties of regional haze dominated by biomass burning aerosol measured from the C-130 aircraft during SAFARI 2000, *J. Geophys. Res.*, 108, 8473, doi:10.1029/2002JD002226, 2003
- Heckel, A., Kim, S.-W., Frost, G. J., Richter, A., Trainer, M., and Burrows, J. P.: Influence of low spatial resolution a priori data on tropospheric NO₂ satellite retrievals, *Atmos. Meas. Tech.*, 4, 1805-1820, doi:10.5194/amt-4-1805-2011, 2011.
- Herron-Thorpe, F. L., Lamb, B. K., Mount, G. H., and Vaughan, J. K.: Evaluation of a regional air quality fore-

- 540 cast model for tropospheric NO₂ columns using the OMI/Aura satellite tropospheric NO₂ product, *Atmos. Chem. Phys.*, 10, 8839-8854, doi:10.5194/acp-10-8839-2010, 2010.
- Irie, H., Boersma, K. F., Kanaya, Y., Takashima, H., Pan, X., and Wang, Z. F.: Quantitative bias estimates for tropospheric NO₂ columns retrieved from SCIAMACHY, OMI, and GOME-2 using a common standard for East Asia, *Atmos. Meas. Tech.*, 5, 2403-2411, doi:10.5194/amt-5-2403-2012, 2012.
- 545 Jacob, D. J., Crawford, J. H., Maring, H., Clarke, A. D., Dibb, J. E., Emmons, L. K., Ferrare, R. A., Hostetler, C. A., Russell, P. B., Singh, H. B., Thompson, A. M., Shaw, G. E., McCauley, E., Pederson, J. R., and Fisher, J. A.: The Arctic Research of the Composition of the Troposphere from Aircraft and Satellites (ARCTAS) mission: design, execution, and first results, *Atmos. Chem. Phys.*, 10, 5191–5212, doi:10.5194/acp-10-5191-2010, 2010.
- 550 Johnson, B. T., Heese, B., McFarlane, S. A., Chazette, P., Jones, A., and Bellouin, N.: Vertical distribution and radiative effects of mineral dust and biomass burning aerosol over West Africa during DABEX, *J. Geophys. Res.-Atmos.*, 113, D00C12, doi:10.1029/2008JD009848, 2008a.
- Johnson, B. T., Osborne, S. R., Haywood, J. M., and Harrison, M. A. J.: Aircraft measurements of biomass burning aerosol over West Africa during DABEX, *J. Geophys. Res.-Atmos.*, 113, D00C06,
555 doi:10.1029/2007JD009451, 2008b.
- Jury M.R. and Winter A.: Warming of an elevated layer over the Caribbean. *Clim Chang.* doi:10.1007/s10584-009-9658-3, 2010
- Kleipool, Q. L., Dobber, M. R., de Haan, J. F., and Levelt, P. F.: Earth surface reflectance climatology from 3 years of OMI data, *J. Geophys. Res.-Atmos.*, 113, D18308, doi:10.1029/2008JD010290, 2008.
- 560 Lamsal, L.N., R.V. Martin, A. van Donkelaar, M. Steinbacher, E.A. Celarier, E. Bucsela, E.J. Dunlea, and J. Pinto: Ground-level nitrogen dioxide concentrations inferred from the satellite-borne Ozone Monitoring Instrument, *J. Geophys. Res.*, 113, D16308, doi:10.1029/2007JD009235, 2008.
- Lamsal, L. N., Martin, R. V., van Donkelaar, A., Celarier, E. A., Bucsela, E. J., Boersma, K. F., Dirksen, R., Luo, C., and Wang, Y.: Indirect validation of tropospheric nitrogen dioxide retrieved from the OMI satellite
565 instrument: Insight into the seasonal variation of nitrogen oxides at northern midlatitudes, *J. Geophys. Res.-Atmos.*, 115, D05302, doi:10.1029/2009JD013351, 2010.
- Lamsal, L. N., R. V. Martin, A. Padmanabhan, A. van Donkelaar, Q. Zhang, C. E. Sioris, K. Chance, T. P. Kurosu, and M. J. Newchurch: Application of satellite observations for timely updates to global anthropogenic NO_x emission inventories, *Geophys. Res. Lett.*, 38, L05810, doi:10.1029/2010GL046476, 2011
- 570 Leitão, J., Richter, A., Vrekoussis, M., Kokhanovsky, A., Zhang, Q. J., Beekmann, M., and Burrows, J. P.: On the improvement of NO₂ satellite retrievals – aerosol impact on the airmass factors, *Atmos. Meas. Tech.*, 3, 475–493, doi:10.5194/amt-3-475-2010, 2010.
- Logan, J. A.: Nitrogen oxides in the troposphere: Global and regional budgets, *J. Geophys. Res.*, 88(C15), 1078510807, doi:10.1029/JC088iC15p10785, 1983
- 575 Ma, J. Z., Beirle, S., Jin, J. L., Shaiganfar, R., Yan, P., and Wagner, T.: Tropospheric NO₂ vertical column densities over Beijing: results of the first three years of ground-based MAX-DOAS measurements (20082011) and satellite validation, *Atmos. Chem. Phys.*, 13, 1547-1567, doi:10.5194/acp-13-1547-2013, 2013.
- Mao, J., Jacob, D. J., Evans, M. J., Olson, J. R., Ren, X., Brune, W. H., St. Clair, J. M., Crouse, J. D., Spencer, K. M., Beaver, M. R., Wennberg, P. O., Cubison, M. J., Jimenez, J. L., Fried, A., Weibring, P., Walega, J.

- 580 G., Hall, S. R., Weinheimer, A. J., Cohen, R. C., Chen, G., Crawford, J. H., McNaughton, C., Clarke, A. D., Jaeglé, L., Fisher, J. A., Yantosca, R. M., Le Sager, P., and Carouge, C.: Chemistry of hydrogen oxide radicals (HO_x) in the Arctic troposphere in spring, *Atmos. Chem. Phys.*, 10, 5823–5838, doi:10.5194/acp-10-5823-2010, 2010.
- Martin, R., Chance, K., Jacob, D., Kurosu, T., Spurr, R., Bucsela, E., Gleason, J., Palmer, P., Bey, I., Fiore, A., Li, Q., Yantosca, R., and Koelemeijer, R.: An improved retrieval of tropospheric nitrogen dioxide from GOME, *J. Geophys. Res.-Atmos.*, 107, 4437, doi:10.1029/2001JD001027, 2002.
- 585 Martin, R., Jacob, D., Chance, K., Kurosu, T., Palmer, P., and Evans, M.: Global inventory of nitrogen oxide emissions constrained by space-based observations of NO₂ columns, *J. Geophys. Res.-Atmos.*, 108(D17), 4537, doi:10.1029/2003JD003453, 2003.
- 590 Mebust, A. K., Russell, A. R., Hudman, R. C., Valin, L. C., and Cohen, R. C.: Characterization of wildfire NO_x emissions using MODIS fire radiative power and OMI tropospheric NO₂ columns, *Atmos. Chem. Phys. Discuss.*, 11, 5351-5378, doi:10.5194/acpd-11-5351-2011, 2011.
- Mebust, A. K., and Cohen, R.C.: Observations of a seasonal cycle in NO_x emissions from fires in African woody savannas, *Geophys. Res. Lett.*, 40, 1451-1455, doi:10.1002/grl.50343, 2013
- 595 Moteki, N., Y. Kondo, Y. Miyazaki, N. Takegawa, Y. Komazaki, G. Kurata, T. Shirai, D. R. Blake, T. Miyakawa, and M. Koike: Evolution of mixing state of black carbon particles: Aircraft measurements over the western Pacific in March 2004, *Geophys. Res. Lett.*, 34, L11803, doi:10.1029/2006GL028943, 2007
- Moteki, N., Y. Kondo, Y.: Method to measure time-dependent scattering cross sections of particles evaporating in a laser beam, *Journal of Aerosol Science*, Volume 39, Issue 4, April 2008, Pages 348-364, 2008
- 600 Oetjen, H., S. Baidar, N. A. Krotkov, L. N. Lamsal, M. Lechner, and R. Volkamer: Airborne MAX-DOAS measurements over California: Testing the NASA OMI tropospheric NO₂ product, *J. Geophys. Res. Atmos.*, 118, 74007413, doi:10.1002/jgrd.50550, 2013
- Osborne, S. R., Johnson, B. T., Haywood, J. M., Baran, A. J., Harrison, M. A. J., and McConnell, C. L.: Physical and optical properties of mineral dust aerosol during the Dust and Biomass-burning Experiment, *J. Geophys. Res.-Atmos.*, 113, D00C03, doi:10.1029/2007JD009551, 2008.
- 605 Palmer, P., Jacob, D., Chance, K., Martin, R., Spurr, R., Kurosu, T., Bey, I., Yantosca, R., Fiore, A., and Li, Q.: Air mass factor formulation for spectroscopic measurements from satellites: Application to formaldehyde retrievals from the Global Ozone Monitoring Experiment, *J. Geophys. Res.-Atmos.*, 106, 14539–14550, doi:10.1029/2000JD900772, 2001.
- 610 Park, R., Jacob, D., Palmer, P., Clarke, A., Weber, R., Zondlo, M., Eisele, F., Bandy, A., Thornton, D., Sachse, G., and Bond, T.: Export efficiency of black carbon aerosol in continental outflow: Global implications, *J. Geophys. Res.-Atmos.*, 110, D11205, doi:10.1029/2004JD005432, 2005.
- Parrington, M., P. I. Palmer, A. C. Lewis, J. D. Lee, A. R. Rickard, P. Di Carlo, J. W. Taylor, J. R. Hopkins, S. Punjabi, D. E. Oram, G. Forster, E. Aruffo, S. J. Moller, S. J.-B. Bauguitte, J. D. Allan, H. Coe, and R. J. Leigh: Ozone photochemistry in boreal biomass burning plumes, *Atmospheric Chemistry and Physics*, 13, pp. 73217341, 2013
- 615 Redelsperger, J., Thorncroft, C. D., Diedhiou, A., Lebel, T., Parker, D. J., and Polcher, J.: African monsoon multidisciplinary analysis – An international research project and field campaign, *B. Am. Meteorol. Soc.*, 87, 1739-1746, doi:10.1175/BAMS-87-12-1739, 2006.

- 620 Reid, J. S., Hyer, E. J., Prins, E. M., Westphal, D. L., Zhang, J., Wang, J., Christopher, S. A., Curtis, C. A., Schmidt, C. C., Eleuterio, D. P., Richardson, K. A., and Hoffman, J. P.: Global Monitoring and Forecasting of Biomass-Burning Smoke: Description of and Lessons From the Fire Locating and Modeling of Burning Emissions (FLAMBE) Program, *IEEE J. Sel. Top. Appl. Earth Observ. Remote Sens.*, 2, 144–162, doi:10.1109/JSTARS.2009.2027443, 2009.
- 625 Reid, J. S., Eck, T. F., Christopher, S. A., Koppmann, R., Dubovik, O., Eleuterio, D. P., Holben, B. N., Reid, E. A., and Zhang, J.: A review of biomass burning emissions part III: intensive optical properties of biomass burning particles, *Atmos. Chem. Phys.*, 5, 827–849, doi:10.5194/acp-5-827-2005, 2005
- Richter, A. and Burrows, J.: Tropospheric NO₂ from GOME measurements, *Remote Sensing of Trace Constituents in the Lower Stratosphere, Troposphere and the Earth's Surface: Global Observations*, Air Poll. 630 *Atmos. Correct.*, 29, 1673–1683, doi:10.1016/S0273-1177(02)00100-X, 2002.
- Rivera, C., Stremme, W., and Grutter, M.: Nitrogen dioxide DOAS measurements from ground and space: comparison of zenith scattered sunlight ground-based measurements and OMI data in Central Mexico, *Atmosfera* 26(3), 401–414, 2013
- Russell, A. R., Perring, A. E., Valin, L. C., Bucsele, E. J., Browne, E. C., Wooldridge, P. J., and Cohen, R. C.: A 635 high spatial resolution retrieval of NO₂ column densities from OMI: method and evaluation, *Atmos. Chem. Phys.*, 11, 8543–8554, doi:10.5194/acp-11-8543-2011, 2011.
- Singh, H. B., Anderson, B. E., Brune, W. H., Cai, C., Cohen, R. C., Crawford, J. H., Cubison, M. J., Czech, E. P., Emmons, L., Fuelberg, H. E., Huey, G., Jacob, D. J., Jimenez, J. L., Kaduwela, A., Kondo, Y., Mao, J., Olson, J. R., Sachse, G. W., Vay, S. A., Weinheimer, A., Wennberg, P. O., Wisthaler, A., and ARCTAS 640 Sci Team: Pollution influences on atmospheric composition and chemistry at high northern latitudes: Boreal and California forest fire emissions, *Atmos. Environ.*, 44, 4553–4564, doi:10.1016/j.atmosenv.2010.08.026, 2010.
- Spurr, R.: Simultaneous derivation of intensities and weighting functions in a general pseudo-spherical discrete ordinate radiative transfer treatment, *J. Quant. Spectrosc. Ra.*, 75, 129–175, doi:10.1016/S0022- 645 4073(01)00245-X, 2002.
- Spurr, R., Kurosu, T., and Chance, K.: A linearized discrete ordinate radiative transfer model for atmospheric remote-sensing retrieval, *J. Quant. Spectrosc. Ra.*, 68, 689–735, doi:10.1016/S0022-4073(00)00055-8, 2001.
- Wiedinmyer, C., X. Tie, A. Guenther, R. Neilson, C. Granier.: Future changes in biogenic isoprene emissions: how might they affect regional and global atmospheric chemistry? *Earth Interactions*, v10, paper 3., 2006
- 650 Zhou, Y., Brunner, D., Boersma, K. F., Dirksen, R., and Wang, P.: An improved tropospheric NO₂ retrieval for OMI observations in the vicinity of mountainous terrain, *Atmos. Meas. Tech.*, 2, 401–416, doi:10.5194/amt-2-401-2009, 2009.
- Zyrichidou, I, Koukouli M.E., Balis D.S., Kioutsoukis I., Poupkou A., Katragkou E., Melas D., Boersma K.F., van Roozendaal M., Evaluation of high resolution simulated and OMI retrieved tropospheric NO₂ column 655 densities over Southeastern Europe, *Atmospheric Research*, Volume 122, Pages 55–66, 2013

Tables

Table 1. DC-8 research payload during ARCTAS-B for the species considered in this study.

Species, parameters	Method	Investigator	Reference
NO ₂	TD-LIF	R. Cohen, UC Berkeley	Cleary et al. (2002)
Aerosol optical properties	Nephelometer, PSPAP	B. Anderson, NASA LaRC	Anderson et al. (1998)
Black carbon aerosol	SP2	Y. Kondo, U. Tokyo	Moteki and Kondo (2007, 2008)

Table 2. FAAM BAe-146 research payload during DABEX for the species considered in this study.

Species, parameters	Instrument	Comment
NO ₂	TECO 42	detection limit < 2 ppbv
Aerosol absorption	Radiance Research PSAP	wavelength, $\lambda = 0.568 \mu\text{m}$
Dry aerosol scattering	TSI 3563 Nephelometer	$\lambda = 0.45, 0.55, 0.70 \mu\text{m}$

Table 3. Simulated and observed mean SSA and AOD columns at several AERONET sites during DABEX.

	SSA	AOD
Banizoumbou (13° N, 2° E)		
AERONET	0.84	0.75
GC	0.84	0.63
Djougou (9° N, 1° E)		
AERONET	0.82	1.05
GC	0.84	1.19
IER-Cinzana (13° N, 5° W)		
AERONET	0.83	0.65
GC	0.85	0.61
Ilorin (8° N, 4° E)		
AERONET	0.86	1.37
GC	0.89	0.80
DMN-Maine Soroa (13° N, 12° E)		
AERONET	0.88	0.80
GC	0.82	1.23
Dakar (14° N, 16° W)		
AERONET	0.83	0.84
GC	0.85	0.95

Figure Captions

Fig. 1. a) NASA DC-8 and b) FAAM BAe-146 flight tracks during ARCTAS-B and DABEX, respectively. The color indicates the altitude of the aircraft. c) map of the AERONET stations considered in this study.

Fig. 2. Simulated and observed vertical profiles of NO₂ shape factors (**a**), aerosol extinction coefficient (440 nm) (**b**), and single scattering albedo (440 nm) (**c**) during ARCTAS, and NO₂ shape factors (**d**), aerosol extinction coefficient (440 nm) (**e**), and aerosol scattering coefficient (440 nm) (**f**) during DABEX. Modeled median values (dashed line) are represented by crosses and observed median values (solid line) by triangles. Modeled mean values are represented by diamonds and observed mean values by square. Bars indicate the standard error of the mean at each altitude level.

Fig. 3. Mean AMF shape factor correction over Canadian fires during ARCTAS (30 June–10 July 2008) (left) and western Africa fires during DABEX (13 January–2 February 2006) (right). Retrievals with a cloud fraction > 5% have been excluded.

Fig. 4. Left: GEOS-Chem aerosol extinction coefficients profile with (solid line) and without (dashed line) the elevated aerosol layer for a single grid cell over west Africa fires at OMI overpass time (13:30 LT). The aerosol correction factor values corresponding to each type of aerosol profile are reported on the figure. Right: GEOS-Chem NO₂ profile shape for the same grid cell.

Fig. 5. Aerosol correction factor sensitivity to: (**a**) single scattering albedo, (**b**) solar zenith angle, (**c**) surface reflectance, and (**d**) emissions (aerosol and NO₂ surface concentration rescaling). Solid and dashed lines correspond to the case with and without the elevated aerosol layer, respectively. For each parameter, the arrow indicates the value corresponding to the reference case.

Fig. 6. Aerosol correction factor sensitivity to cloud fraction for different AODs. Left: case with an elevated aerosol layer. Right: case with a surface-only aerosol layer. Different AODs were obtained by rescaling either the elevated aerosol layer (left panel) or the surface aerosol layer (right panel).

Fig. 7. Shape factor correction sensitivity to cloud fraction (left) and surface reflectance (right). The arrow indicates the surface reflectance value corresponding to the reference case.

Fig. 8. Relationship between the NO₂ correction factor and ΔNO_2 . Vertical bars represent the standard deviation of the NO₂ correction factor within each ΔNO_2 bin. The solid black line represents the logarithmic fit to the curve.

Figures

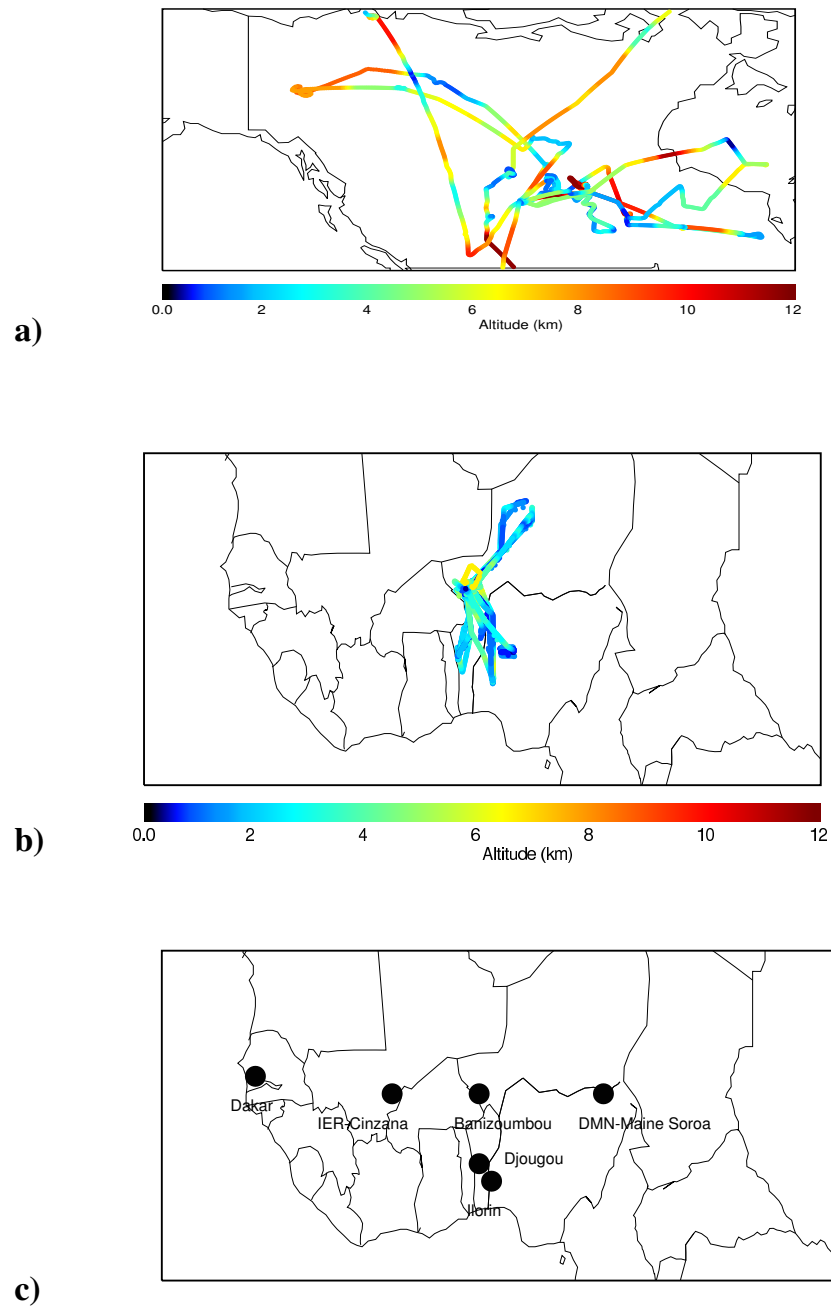


Fig. 1. a) NASA DC-8 and b) FAAM BAe-146 flight tracks during ARCTAS-B and DABEX, respectively. The color indicates the altitude of the aircraft. c) map of the AERONET stations considered in this study.

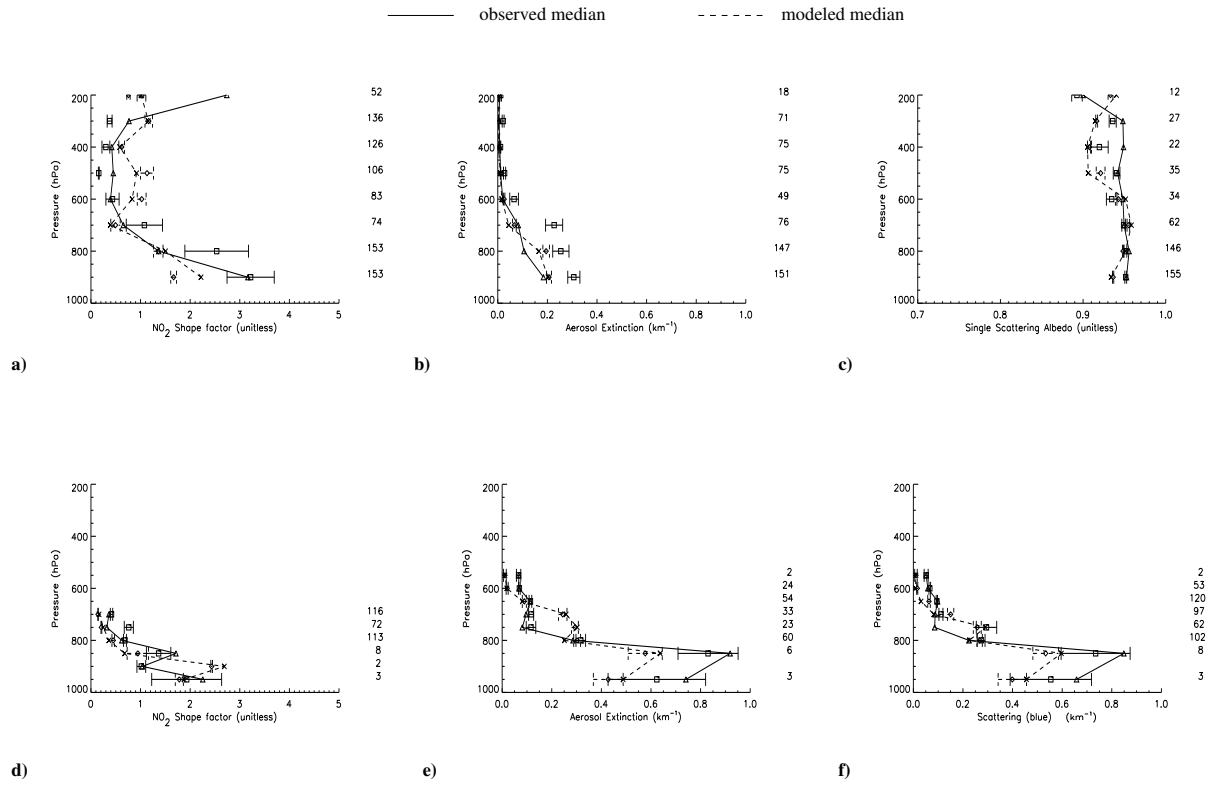


Fig. 2. Simulated and observed vertical profiles of NO₂ shape factors (a), aerosol extinction coefficient (440 nm) (b), and single scattering albedo (440 nm) (c) during ARCTAS, and NO₂ shape factors (d), aerosol extinction coefficient (440 nm) (e), and aerosol scattering coefficient (440 nm) (f) during DABEX. Modeled median values (dashed line) are represented by crosses and observed median values (solid line) by triangles. Modeled mean values are represented by diamonds and observed mean values by square. Bars indicate the standard error of the mean at each altitude level.

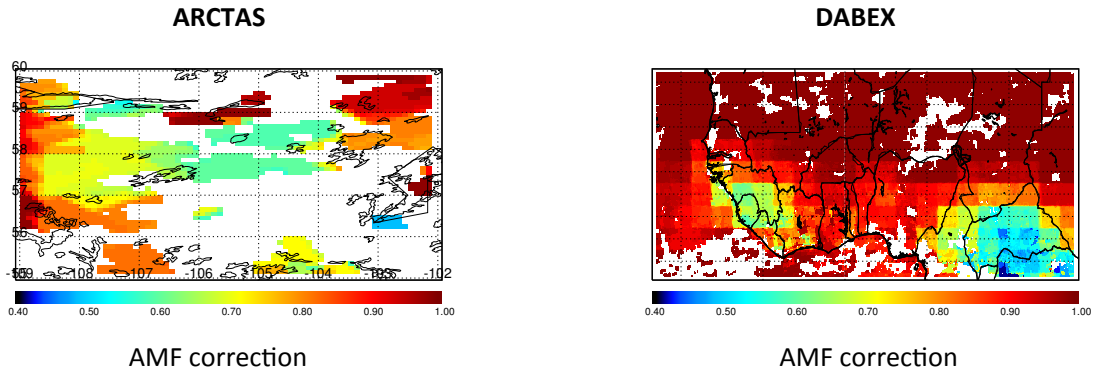


Fig. 3. Mean AMF shape factor correction over Canadian fires during ARCTAS (30 June–10 July 2008) (left) and western Africa fires during DABEX (13 January–2 February 2006) (right). Retrievals with a cloud fraction $> 5\%$ have been excluded.

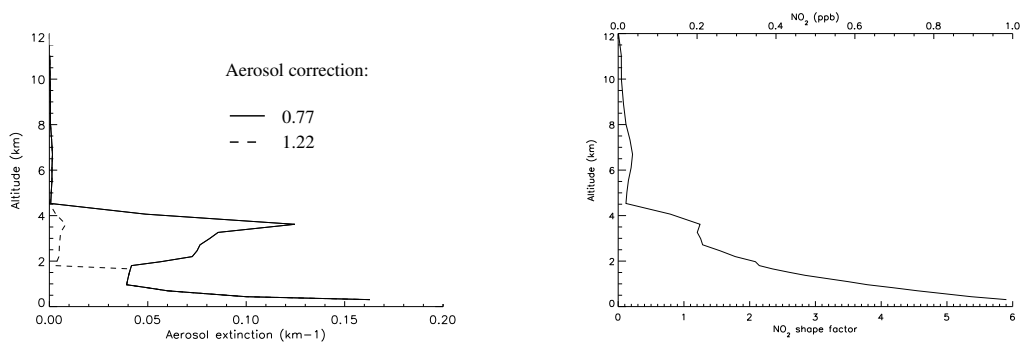


Fig. 4. Left: GEOS-Chem aerosol extinction coefficients profile with (solid line) and without (dashed line) the elevated aerosol layer for a single grid cell over west Africa fires at OMI overpass time (13:30 LT). The aerosol correction factor values corresponding to each type of aerosol profile are reported on the figure. Right: GEOS-Chem NO_2 profile shape for the same grid cell.

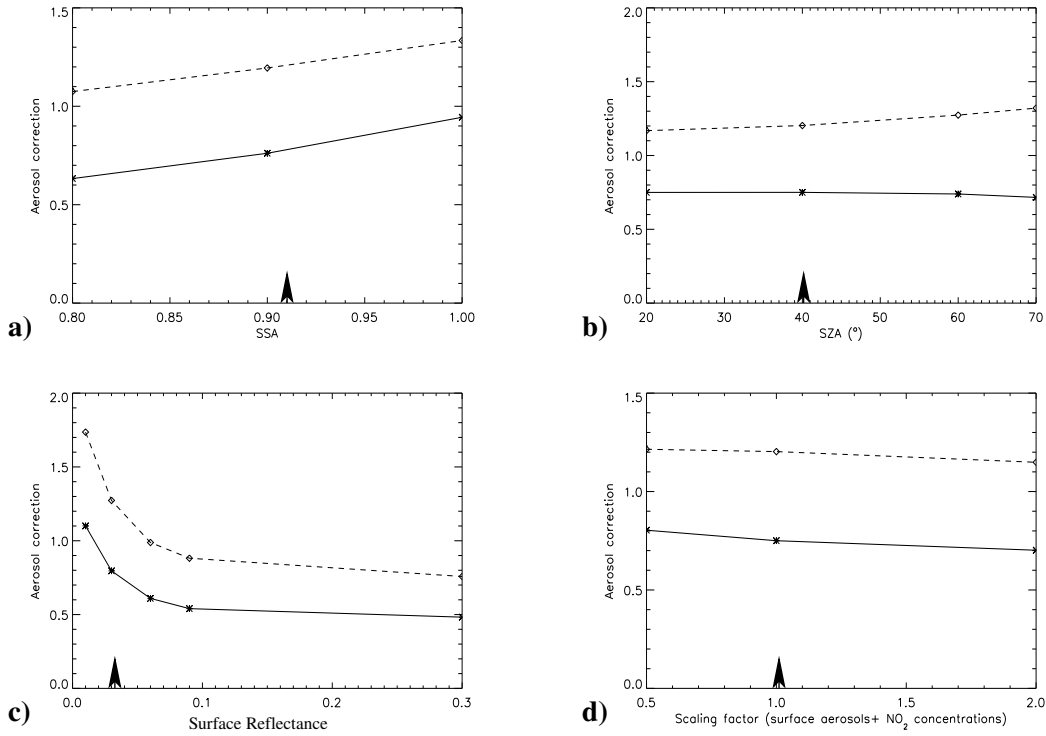


Fig. 5. Aerosol correction factor sensitivity to: **(a)** single scattering albedo, **(b)** solar zenith angle, **(c)** surface reflectance, and **(d)** emissions (aerosol and NO₂ surface concentration rescaling). Solid and dashed lines correspond to the case with and without the elevated aerosol layer, respectively. For each parameter, the arrow indicates the value corresponding to the reference case.

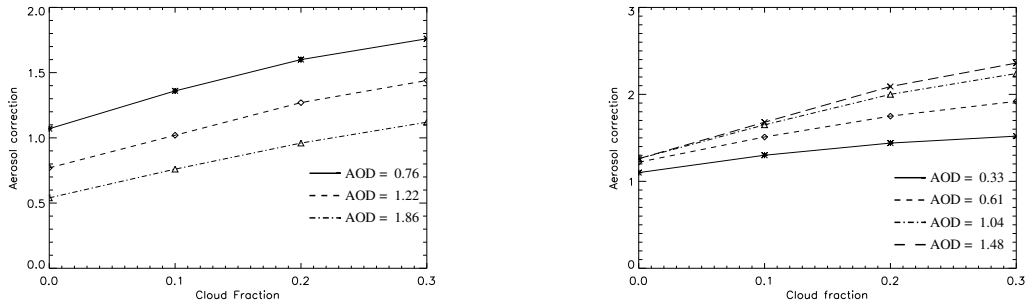


Fig. 6. Aerosol correction factor sensitivity to cloud fraction for different AODs. Left: case with an elevated aerosol layer. Right: case with a surface-only aerosol layer. Different AODs were obtained by rescaling either the elevated aerosol layer (left panel) or the surface aerosol layer (right panel).

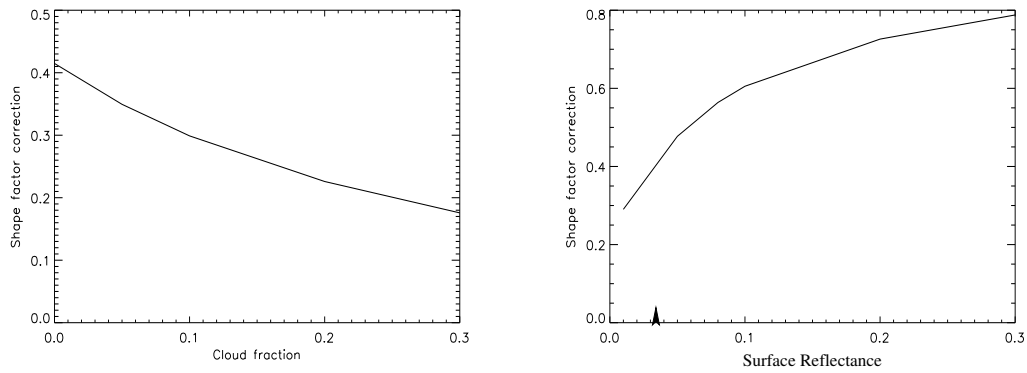


Fig. 7. Shape factor correction sensitivity to cloud fraction (left) and surface reflectance (right). The arrow indicates the surface reflectance value corresponding to the reference case.

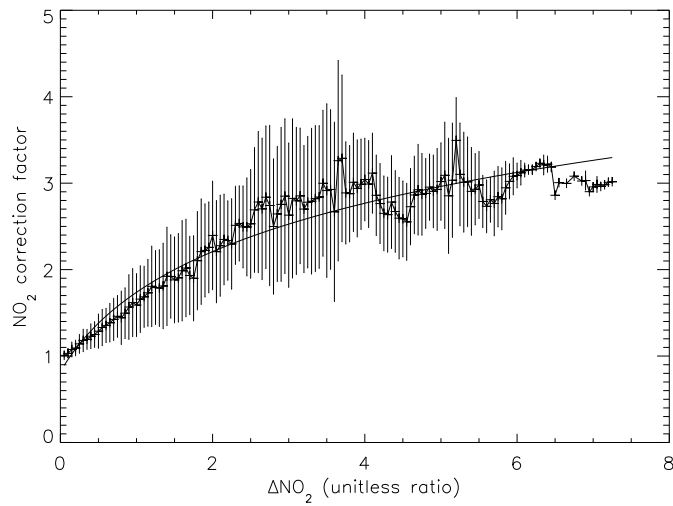


Fig. 8. Relationship between the NO_2 correction factor and ΔNO_2 . Vertical bars represent the standard deviation of the NO_2 correction factor within each ΔNO_2 bin. The solid black line represents the logarithmic fit to the curve.